Energy Systems
https://doi.org/10.1007/s12667-023-00612-0

ORIGINAL PAPER

# An approach to evaluating the impact of contaminants on flux deposition in gas turbines

**Stefano Mori[1] · Mathilde Mendil[1] · Jonathan Wells[2] · Neil Chapman[2] · Nigel Simms[1] · Roger Wells[2] · Joy Sumner[1]**

Received: 27 June 2023 / Accepted: 31 July 2023


## Abstract

Gas turbines are a key part of many countries' power generation portfolios, but components such as blades can suffer from hot corrosion attack, which can decrease component lifetimes. Corrosion is driven by impurity levels in the fuel and air (e.g., species containing sulphur and/or alkali metals) and depends on environmental conditions (e.g., air pollution, seawater droplets), that can lead to formation of harmful species in the gas. Understanding and determining the deposition flux of such contaminants is crucial for understanding the problem. Thermodynamic simulations were used to determine types and amounts of potentially corrosive contaminants, this was followed by deposition fluxes calculations. An operating scenario, based upon an offshore platform was evaluated. The effectiveness of different filtration systems has been evaluated. The impurity levels of alkali metals, such as sodium, greatly impacts the calculated deposition flux of species linked to corrosion attack. The presence of $Na_2SO_4$, and $K_2SO_4$ was found, at temperature representative of stage 2 nozzle guide vanes. Lowering sulphur input (from fuel or air) can be an efficient way to decrease deposition, attention must also be paid to lowering the amount of alkali metal entering the gas turbine, which can be lowered by the filtration systems' correct use.

**Keywords** Gas turbine · Turbine blades · Condensation · $Na_2SO_4$ · Air filtration · Sea salt aerosol

✉ Stefano Mori
Stefano.mori@cranfield.ac.uk

[1] Energy and Sustainability, School of Water, Environment Energy and Agrifood, Cranfield University, Cranfield, UK

[2] Siemens Energy, Waterside South, Lincoln LN5 7FD, UK

Published online: 18 August 2023

## 1 Introduction

Gas turbines' contribution to the UK's energy mix has been estimated to account for about 31.8 GW (30%) of electricity production in 2021 [1]. Moreover, annual sales of natural gas represent around $8 billion, and continuous growth has been predicted for the next 10 years [2]. Gas turbines are used in Combined Cycles Gas Turbine power plants (CCGT), which integrate steam turbines, to use waste heat from the gas turbine's exhaust to convert additional energy [3]. This synergy reduces the amount of fuel required per unit of power generated, and so the emission of pollutants per unit energy ($CO_2$, $NO_X$, etc.) also falls compared to a stand-alone gas turbine or a conventional coal-fired plant, which operates at lower temperature hence at lower efficiency, or simple gas turbines which have higher heat losses [4, 5]. In addition, CCGT is very flexible in terms of the fuels that could be utilised [3].

When gas turbine materials are in direct contact with the hot gas stream from fuel combustion, they experience very high degradation rates [6] [7]. This is due to the presence of gaseous impurities, such as $Na_2SO_4$ in the hot gas stream that can condense on the surfaces of gas turbine components as turbine blades are cooler with respect to the gas stream temperature. The condensation of such corrosive species can lead to hot corrosion which has been shown to have two peaks, one around 700 °C and a second one around 850 °C [8].

Gas turbines are complex devices that are composed of different parts, which all play a vital role in the function of the gas turbine. Air and fuel inputs are compressed and then combusted. The combusted gases then pass into the turbine, expanding and turning rotors to convert the energy into electricity. Turbines are composed of several sections, which all operate at different temperatures and pressures, requiring different materials for the different stages. The focus of this work is the nozzle guide vanes (NGV) and blades in the first two stages.

To model the behaviour and simulate the environment in a typical gas turbine, it is necessary to take into account those components, such as filtration system which can reduce contaminants levels. The specification of the environment influenced by fuel and air composition is very important. The use of filtration systems is not only fundamental to stopping particles entering the turbine, but also helps decrease the number of harmful species that could condense and lead to high temperature degradation (e.g. hot corrosion) of the machinery.

Ash particles and vapours are the result of fuel combustion and can cause problems when they deposit on metals' surface. Vapour condensation is the main concern in natural gas combustion. This type of deposition usually occurs on turbine blades surfaces since they are cooler than the surrounding gas environment. Even thin layers of molten mixed deposits can be problematic; fluxing away protective layers in a process known as hot corrosion [9]. These deposits can be in form of alkali chlorides (NaCl, KCl); alkali sulphates ($Na_2SO_4$, $K_2SO_4$); and acidic sulphates ($H_2SO_4$) [10]. The extent to which these compounds can form is dependent upon trace contaminants in the air and fuel, and so simulating these and the resulting post-combustion environments is crucial to understand the hot corrosion

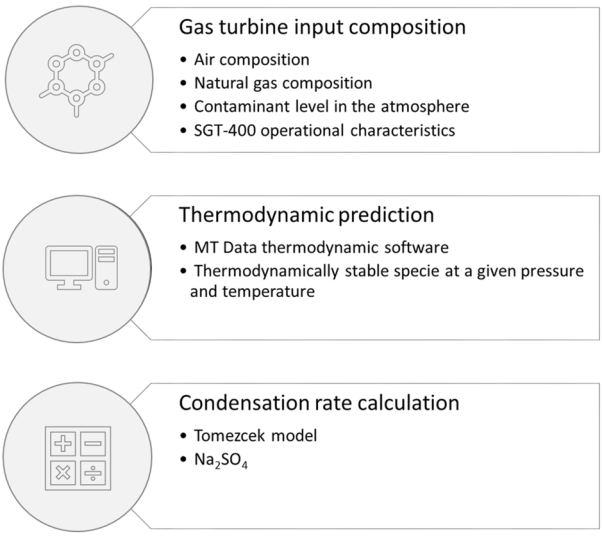


**Fig. 1** Methodology

**Table 1** 13 MW model gas turbine parameters (supplied by Siemens Energy)

| Power output | 13 MW |
|---|---|
| Efficiency | 34.80% |
| Pressure ratio | 16.8:1 |
| Exhaust mass flow | 39.4 kg/s |
| Exhaust temperature | 555 °C |

attack mechanism and so predict turbine component lifetimes. To be able to perform an analysis of anticipated deposit chemistries and fluxes, an understanding of fuel and air specifications (i.e., contaminants levels), as well as air filtration systems is needed.

## 2 Methodology

The methodology used for this work is depicted in Fig. 1. More information has been reported in the Theory section. The parameters used to simulate the turbine are summarised in Table 1. The main parameters used for the simulation are the power output, pressure ratio, mass flow, gas temperature.

The air composition used for the thermodynamic calculations is given in Table 2. In addition to these main components, sea salt aerosol (SSA) particles, as well as dust particles, have been added to the air input for the thermodynamic calculations, as explained in the sections below.

**Table 2** Composition of standard air [11]

| Component | Molar fraction |
|---|---|
| $N_2$ | 0.7809 |
| $O_2$ | 0.2095 |
| Ar | 0.0093 |
| $CO_2$ | 0.0003 |

Parameters such as gas density and dynamic viscosity were assumed to have the same values in the combustion gas as for atmospheric conditions. For this study, these parameters are needed for specific temperatures, hence a curve fitting was made using the data from [12]. The density of exhaust gas $\rho$ in kg/m$^3$ and the dynamic viscosity of the exhaust gas $\mu$ in Pa.s are given in Eqs. (1) and (2), with a correlation factor of 1 for both. In the equation T is temperature in °C.

$$\rho = \frac{349.17}{T} \tag{1}$$

$$\mu = -1 \times 10^{-14} T^3 - 4 \times 10^{-11} T^2 + 7 \times 10^{-8} T + 1 \times 10^{-6} \tag{2}$$

### 2.1 Sand and dust in offshore environment modelling

Sand from deserts can be carried offshore over thousands of kilometres through wind action [13], with the sand's composition dependant on the location of the desert. However, typically, sand is made of different oxides, such as silicon ($SiO_2$), aluminium ($Al_2O_3$), calcium (CaO), iron ($Fe_2O_3$), magnesium (MgO) and potassium ($K_2O$) [13].

Sand particles carried by the wind have a variety of sizes, ranging from 0.01 to 100 µm [14, 15]. Kaaden et al. [15] conducted a study on dust from the Saharan desert to investigate the size distribution, the hygroscopic growth of the Saharan aerosol for background conditions and dust events [15]. He also found that the geometric mean diameter (GMD) for Saharan dust particles was 715 nm during a dust event and 570 nm for the Saharan background aerosol [15]. In addition, it was highlighted that between 30 and 250 nm particles are hygroscopic (usually rich in sodium chloride, sulphates, ammonium sulphate) while over 350 nm particles are hydrophobic (those are composed by iron-rich, titanium-rich, quartz, calcium carbonates, gypsum, carbonaceous species, silicates) [15]. Schütz et al. [16] noticed, that during atmospheric transport, the mean value of the particle size distribution decreases. This is likely because gravitational settling preferentially removes larger particles [16].

Stohl [17] gathered data showing that dust particles can be coated with sulphates. This is particularly the case in polluted regions such as the Mediterranean area or eastern China. The pollutant are absorbed by the particles (e.g. sea salt, dust) on their surface forming salts ($Na_2SO_4$, $NaNO_3$, $CaSO_4$, $Ca(NO_3)_2$) [18, 19]. However, sulphates

are also found on the dust particles on the Saharan desert, but those could be mainly ascribed to sulphate in mineral form, which does not react inside the gas turbine [17]. These form the basis of inputs for sand in later calculations.

### 2.2 Filtration systems and filter efficiency

Gas turbines are equipped with filtration systems to decrease the amount of contaminants ingested with inlet air [20]. Gas turbines manufacturers provides recommended criteria for air quality. Filters are chosen to meet, at a minimum, these criteria; their choice depends on the specific operational location of the gas turbine [21].

Therefore, the first step in the choice of a filtration system is to define the operational environment. Location for the turbine has been assumed as "coastal, marine, or offshore". Gas turbine components can be sensitive to solid particles, liquid contaminant and gas contaminant [13].

#### 2.2.1 Filtration curves

In this work two filtration systems were considered, following the European standard BS EN 779:2012 [22] and BS EN 1822–1:2019 [23]: Standard: G2, M6, E11 and High efficiency: G2, F6, E12.

A filter's efficiency is a ratio of captured particle quantity (weight, volume or number) over the inlet particle quantity, Eq. (3) [24].

$$\eta = \frac{W_{entering} - W_{leaving}}{W_{entering}} \tag{3}$$

**Table 3** Parameters used for the different simulations

| Scenario | Fuel | Air | Contaminant | Normalised S | Normalised Saharan dust | Normalised seal salt |
|---|---|---|---|---|---|---|
| A | Dirty | Standard | $H_2S$ 5 ppm | 17.20 | – | – |
| B– G2, M6 | Dirty | Standard – G2, M6 | $H_2S$ 50 ppm + Sea salt aerosol | 18.28 | – | REF |
| B– HEPA[1] | Dirty | Standard – HEPA | $H_2S$ 50 ppm + Sea salt aerosol | 18.26 | – | 0.103 |
| C – G2, M6 | Dirty | Standard – G2, M6 | $H_2S$ 50 ppm + Sea salt aerosol + Saharan dust | 18.28 | REF | 1 |
| C– HEPA[1] | Dirty | Standard – HEPA | $H_2S$ 50 ppm + Sea salt aerosol + Saharan dust | 18.26 | 0.059 | 0.103 |

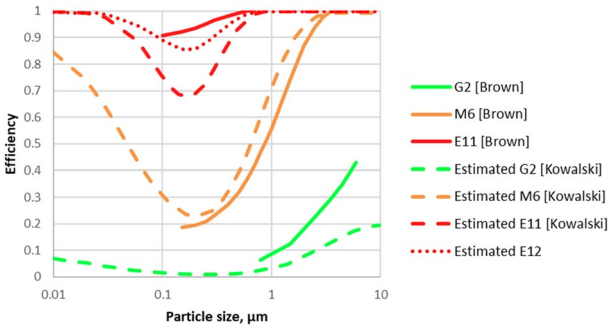


**Fig. 2** Sum of sea-salt size log-normal distribution for film, jet and spume drop mode

**Table 4** Tri modal lognormal distribution parameters [32]

| | Film drop | Jet drop | Spume drop |
|---|---|---|---|
| GM | 0.1 | 1 | 6 |
| GSD | 1.9 | 2 | 3 |

**2.2.1.1 Scenario assumptions** This study will focus on a gas turbine located on an offshore field in the Arabian Gulf, 180 km away from Abu Dhabi (Abu Al Bukhoosh; ABK). Six different scenarios have been simulated; they are listed in Table 3.

Dust was assumed to come from the Saharan desert, known as 'Harmattan' dusts, and the composition was measured in Spain [25]. As Saharan dust contains minerals, such as clay or glass, which do not react in the gas turbine, only the water-soluble species were considered in the study. A study led by Alebić-Juretić et al. on a Saharan dust event on 12th of April in 2002 recorded the water-soluble ions contained in the dust [26]. To do that, the ions were measured in the deposit sediment in Croatia. It was found that the weight fraction of $SO_4^{2-}$ from deposited dusts was about 0.039%. The dust concentration used was 15,000 mg/m$^3$, which corresponds to the concentrations found during a dust event [27]. Concerning the dust particle size for this study, the geometric mean (GM) was 0.5 nm, and the geometric standard deviation (GSD) was 1.9 nm [27] (Fig. 2).

The amount of salt entering the turbine and the dust coming from the land conveyed by wind were taken into account. Then, the salt passes through the filtration system. With a wind speed of 10 m/s and a 14 m height location, 93%, 7% and 0.00004% of SSA is respectively in film drop, jet drop and spume drop mode. The parameters of the lognormal size distribution of each mode are given in Table 4. The size distribution obtained is shown in Fig. 2.

The composition of the SSA has been assumed to be the same of sea water, in the Persian Gulf water, given in Table 5 [33]. The gas turbine in this scenario also experiences high variation in the quality of the gas supplied. Hence, two types of fuel were simulated, one being "standard gas" and the other, "dirty gas" (Table 6).

It was assumed that the air entering the gas turbine had a molar volume as an ideal gas at 0 °C and P = 1°atm. This would have an impact on the amount

**Table 5** Salt content in Persian Gulf water [33]

| Component | Content (wt. ppm) |
|---|---|
| Ca | 419 |
| Mg | 1304 |
| Na | 10,710 |
| K | 390 |
| $SO_4^{2-}$ | 2690 |
| Cl | 19,350 |

**Table 6** Composition the "standard gas" and the 'dirty gas" [34]

| Component | Standard gas (molar fraction) | Dirty gas (molar fraction) |
|---|---|---|
| $CH_4$ | 0.942 | 0.841 |
| $C_2H_6$ | 0.032 | 0.043 |
| $C_3H_8$ | 0.006 | 0.015 |
| i-$C_4H_{10}$ | 0.001 | 0.003 |
| n-$C_4H_{10}$ | 0.001 | 0.005 |
| i-$C_5H_{12}$ | 0.001 | 0.002 |
| n-$C_5H_{12}$ | – | 0.002 |
| $C_6H_{14}$ | – | 0.002 |
| $C_7H_{16}$ | – | 0.001 |
| $CO_2$ | 0.005 | 0.03 |
| $N_2$ | 0.012 | 0.036 |
| $H_2S$ | 0.0012 | 0.0205 |

of contaminants (dust, SSA) entering the gas turbine, along with the air. The formula given in Eq. (4) give the molar volume ($V/n$) depending on the temperature [28].

$$\frac{V}{n} = \frac{RT}{P} \tag{4}$$

where V is the volume in $m^3$, n is the amount in mol, R is the ideal gas constant equals to 8.314 J/K/mol, T is the temperature in K, and P is the pressure fixed at 101,325 Pa (1 atm).

The saturation pressure ($p_{sat,A}$) was estimated using MTData, through the calculation of the Gibbs' free energy ($\Delta G$) of the phases. For the calculations it was assumed that the temperature of the bulk gas is fixed. Only the metal temperature varies. As nitrogen is the most abundant species, it is assumed that the coefficient $D_{A,N_2}$ describe the diffusion coefficient of the species A through the hot gas stream [10].

## 3 Theory

Some background theory has been used to perform this work, starting from the vapour condensation model to filtration efficiency, to SSA concentration and particle distribution. The main point of the background used can be found in this section.

## 4 Vapour condensation models

Tomeczek et al. [29] proposed a method to model deposit growth from aerosols, ashes and vapours, that could be found in combusted environment, on a cooled boiler tube. The work focused on deposition of $Na_2SO_4$ and $K_2SO_4$ compounds [29]. This method predicts the rate of condensation of the species A, $\dot{m}_{c,A}$ in kg/s/m$^2$, following Eq. (5).

$$\dot{m}_{c,A} = B_A \frac{p_A - p_{sat,A}}{P} \rho_g \tag{5}$$

where $B_A$ is the mass transfer coefficient (m/s), $p_A$ is the partial pressure of the species A (Pa), $p_{sat,A}$ is the saturation pressure (or vapour pressure) of the species A (Pa), $\rho_g$ is the gas density (kg/m$^3$), and $P$ is the total pressure (Pa). The mass transfer coefficient $B_A$ (m/s) is given by Eq. (6).

$$B_A = \frac{ShD_{A,B}}{D} \tag{6}$$

where $D_{A,B}$ is the diffusion coefficient of species A through species B (m$^2$/s), D is the tube diameter (m), and $Sh$ is the Sherwood number depending on Reynolds number ($Re$) and Schmidt Number ($Sc$).

Usually for combustion systems, it is assumed that nitrogen is the most abundant species in the hot gas stream. Hence, it is assumed for the calculation that the coefficient $D_{A,N_2}$ describe the diffusion coefficient of the species A through the hot gas stream [10].

The saturation pressure (or vapour pressure) of the condensing species A, $p_{sat,A}$, depends on the gas temperature. Tomeczek et al. approximated this using Antoine's equation, Eq. (7) [29].

$$\frac{p_{sat,A}}{p_n} = \exp\left(A - \frac{B}{T_s + C}\right) \tag{7}$$

where A, B and C are Antoine equation parameters, and T is the temperature (K).

## 5 Sea salt aerosol modelling

Sea salt can be found in air as aqueous aerosol or solid particles [21]. SSA is a mixture of very small particles or droplets of salt in the air. Anything that affects the seawater's surface may impact SSA properties, such as atmospheric stability, sea

temperature, air temperature, rainfall, sea topography, etc. [30]. Wind has a major impact on SSA concentration as it causes waves to break, and it affects the upward transport of SSA in the air [30]. It is usually measured at 10 m above the sea surface (and called $U_{10}$).

SSA particles are typically divided into three principal subgroups based on their geometric radius at a relative humidity of RH = 80% ($r_{80}$) [31]:

- Small SSA particles ($r_{80} \leq 0.1$–1 µm)
- Medium SSA particles (1 µm < $r_{80}$ < 25 µm)
- Large SSA particles ($r_{80} > 100$ µm)

Moreover, three modes of formation of a SSA were highlighted by O'Dowd et al. [32]: film drop (0.2–0.4 µm diameter), jet drop (2–4 µm diameter) and spume drop mode (up to 200 µm diameter). In their paper [32], they found that the particle size distribution can be described by a tri-modal lognormal curve, which parameters are defined in Table 4.

In addition, the total concentration ($cm^{-3}$) for each mode could be calculated by Eqs. (8), (9) and (10), where $U_{10}$ is the wind speed at 10 m height (m/s).

$$\log(N_{film}) = 0.095U_{10} + 0.283 \tag{8}$$

$$\log(N_{jet}) = 0.0422U_{10} - 0.288 \tag{9}$$

$$\log(N_{jet}) = 0.0422U_{10} - 0.288 \tag{10}$$

The SSA composition depends directly on the composition of the sea, for the reason it might differ from one region to another, depending on the location on earth. Despite the difference in composition, the main species that could be found in SSA are alkali metals, such as sodium, magnesium, calcium, potassium, chloride, sulphate, etc. The simultaneous presence of these alkali compounds along with sulphur compounds (coming from the air or the fuel) may be detrimental to the gas turbine, and might lead to hot corrosion occurrence on the hot gas path section [13].

## 6 Calculations

The calculations based on the theoretical background of the previous sections are explained below.

## 7 Calorific value calculations

The calorific value of the fuel was calculated based on ISO 6976 (1995) [35], taking into account each molecule constituting the natural gas used for the study. From that, the fuel mass flow ($\dot{m}_{fuel,input}$ in kg/s) was calculated using Eq. (11)

**Table 7** Calculated characteristics of the gas turbine

| | |
|---|---|
| Air-to-fuel ratio | 30 |
| Input fuel mass flow | 0.78 kg/s |
| Fuel calorific value | 48.16 MJ/kg |

$$\dot{m}_{fuel,input} = \frac{Power}{Efficiency \times Calorificvalue} \tag{11}$$

where the power of the gas turbine is in J/s and the calorific value in kg/s. Afterwards the air mass flow rate ($\dot{m}_{air,input}$ in kg/s) was deduced using Eq. (12).

$$\dot{m}_{air,input} = \dot{m}_{fuel,input} \times \text{air-to-fuel ratio} \tag{12}$$

For calculation purposes it was assumed that air has a molar volume of 22.4 L/mol, which is the standard value for ideal gas at 1 atm and 0 °C. The results of this calculations are reported in Table 7.

## 8 Vapour condensation calculations

The rate of condensation (flux) of the species A (kg/s/m$^2$) was calculated using Eq. (5) from Tomeczek's model [29]. The mass transfer coefficient $B_A$ (m/s) was calculated using Eq. (6), and the diffusion coefficients for gases and vapours species were estimated using the Gilliland model [36]. The Reynolds number was calculated using Eq. (13) and the Schmidt number using Eq. (14).

$$Re = \frac{V_g L \rho_g}{\mu_g} \tag{13}$$

$$Sc = \frac{\mu_g}{\rho_g D_{A,B}} \tag{14}$$

where $V_g$ is the speed of the exhaust gas (m/s), L is a characteristic length (m), $\mu_g$ is the dynamic viscosity (Pa.s), $\rho_g$ the density of the fluid (kg/m$^3$) and $D_{A,B}$ is the diffusion coefficient of species A through species B (m$^2$/s).

Then, the Sherwood number, was calculated following Kutatela's method, for a flow normal to a cylinder and for a Schmidt number over 0.5 [37] (Eq. (15)) using Eq. (16).

$$Sh = A \times Sc^{0.37} \times Re^m \tag{15}$$

$$Sc \geq 0.5 \tag{16}$$

where the coefficients A and m depend on the Reynolds number [37].

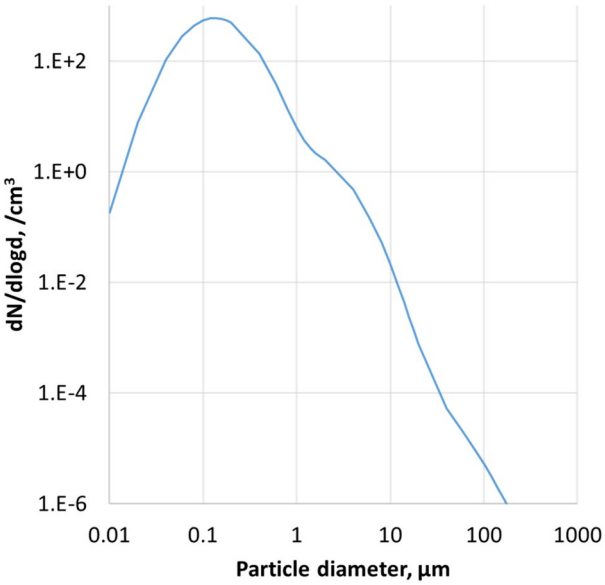


**Fig. 3** Composite of efficiency curve from different sources for filters G2, M6, E11 and E12 [36, 39]

## 9 Filter efficiency calculations

Filter efficiency from this study is an assembly of information from different sources, represented in Fig. 3. Brown tested filter efficiency with ASHRAE filters from 0.1 to 10 µm [38] and Kowalski and Bahnfleth tested European filters from 0.01 to 10 µm [39]. The efficiency curve of E12 was estimated to fit the standards. In addition, these efficiency curves represent the worst-case situation, as filters are new, hence the efficiency is lower compared to that expected in operation, when it gets clogged with time [40]

## 10 Sea salt aerosol calculations

Many models have been developed to predict SSA concentration depending on wind speed [41]. Yoshiaki [42] proposed a model to predict the sea salt concentration taking into account the speed of the wind and the altitude, described in Eq. (17):

$$s = 5 \times \left(6.3 \times 10^{-6} \times H\right)^{0.21-\log(W)} \tag{17}$$

where s is the SSA concentration in µg/m$^3$, W is the wind speed in m/s and H is the altitude above the sea level in m. For this work it has been assumed the gas turbine and the filtration system are about 14 m above sea level on an offshore platform.

## 11 Results and discussion

This section presents condensation data for different scenarios, different stages inside the turbine, and different filter efficiencies. Among the different species found through the thermodynamic modelling, this work will focus mainly on the condensation of $Na_2SO_4$.

## 12 Vapour condensation

The only condensed and deposited species found (through MTData thermodynamic modelling) in this scenario are $MgSO_4$, $CaSO_4$, $K_2SO_4$ and $Na_2SO_4$. Between the temperature of stage 2 blades and stage 1 NGV (Table 8), only $K_2SO_4$ and $Na_2SO_4$ were able to melt; these are both species of interest from a hot corrosion point of view. The two other species remain as solid particles. $Na_2SO_4$ condensation fluxes are shown in Fig. 4. In Fig. 4 the metal temperature of the stage 2 blades has been taken as reference point (X) and all the temperature are expressed as a difference from X. This has been done due to the sensitivity of the metal temperature data.

The cases B and C having the same filtration system (G2 and M6) show $Na_2SO_4$ condensation fluxes that almost overlap (only 0.0001% of difference), no matter the difference of sulphur input (0.002% difference between B and C sulphur). The observation is the same for the case B and C with HEPA filters. This validates the finding that sulphur is in excess in the turbine. High efficiency filtration systems (ie. HEPA) cause a decrease of $Na_2SO_4$ condensation fluxes by a factor of 2, resulting in a deposition flux of 2.15 μg/cm$^2$/h (HEPA) compared with 4.85 μg/cm$^2$/h for G2, M6.

Condensation fluxes were plotted (Fig. 5) for the 2 stages of NGVs and blades. These results indicate the fluxes of condensation was greatest on the stage 2 NGV with the G2 M6 filtration system followed by that of the stage 1 blade and then the stage 2 blade, both with the G2 M6 filtration. For the stage 1 NGV, there is no condensation of $Na_2SO_4$ recorded with HEPA filtration system, and the rates of condensation with G2, M6 filters are too low (0.006 μg/cm$^2$/h at X-190 K) to display clearly

**Table 8** $Na_2SO_4$ flux of condensation at the stage 1 and 2 NGVs and blades with the G2, M6 and HEPA filtration system. Note, metal temperatures supplied by Siemens Energy but due to the sensitivity of this data, the temperatures are not repeated in this paper

| | Filtration system | Metal temperature (K) | $Na_2SO_4$ condensation rate (μg/cm$^2$/h) |
|---|---|---|---|
| Stage 1 NGV | G2, M6 | X + 100 | – |
| | HEPA | | – |
| Stage 1 blades | G2, M6 | X + 50 | 1.37 |
| | HEPA | | – |
| Stage 2 NGV | G2, M6 | X | 3.08 |
| | HEPA | | 0.18 |
| Stage 2 blades | G2, M6 | X | 0.84 |
| | HEPA | | 0.53 |

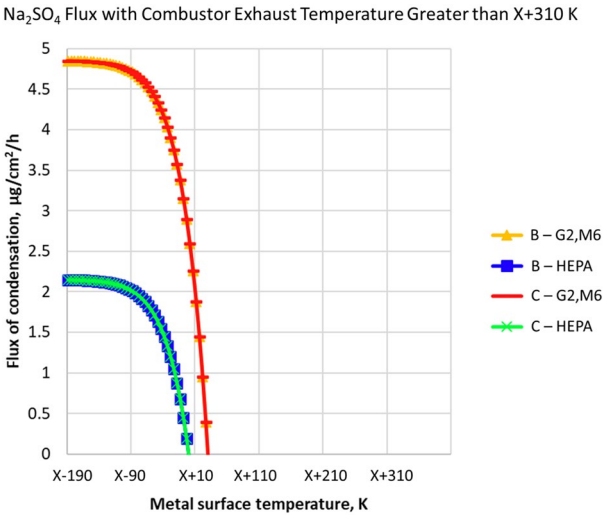


**Fig. 4** Flux of condensation of $Na_2SO_4$, at $T_{gas} = (X\text{-}109)$ K and p = 1 atm. The different curves represent the different filtering systems (standard and HEPA) for Scenario B (dirty fuel plus contaminants and sea salts) and Scenario C (dirty fuel plus contaminants, sea salt and Saharan dust). The combustor exhaust temperature is greater than X + 310 K

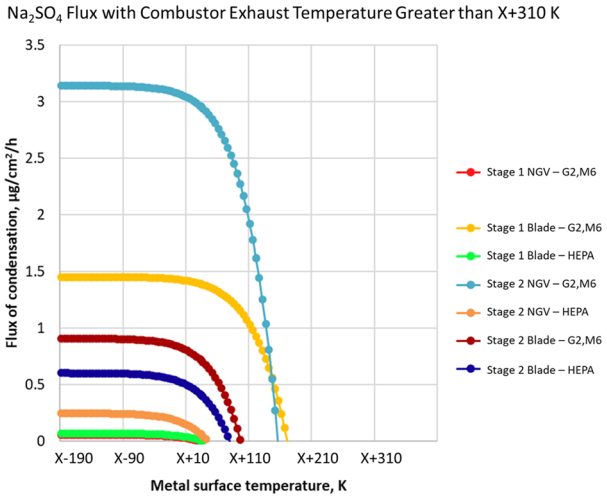


**Fig. 5** Flux of condensation, for scenario C, of $Na_2SO_4$ on the stage 1 and 2 NGVs and blades with different filtration systems. The combustor exhaust temperature is greater than X + 310 K

on the graph. Table 8 summarises the rates predicted by the simulations at the blade temperature of each stage. Table 8 indicates that no condensation of $Na_2SO_4$ would occur on the stage 1 NGV components whilst using either the G2 M6 or HEPA filtration systems. For the stage 1 blade, the stage 2 NGV and the stage 2 blades, the

predictions suggest that the HEPA filtration system will minimise the $Na_2SO_4$ condensation and thus reduce the risk of hot corrosion.

The dew points are also different depending on the filtration system used and the stages of the turbine studied. This is summarised in Table 9. The dew point depends on the $Na_2SO_4$ partial pressure but also on the gas temperature. The partial pressure of $Na_2SO_4$ is the highest at the stage 1 blades (stage 1 blades: $1.41 \times 10^{-6}$ Pa for G2, M6 filters, stage 2 NGV: $1.04 \times 10^{-6}$ Pa) of the gas turbine, but fluxes of condensation are higher at the stage 2 NGV because the bulk gas temperature is lower (temperatures not quoted at the request of Siemens Energy).

## 13 Filter efficiency

Filtration curves are not universal, as they depend on the operational velocity of coming air, on humidity level or on the manufacturer itself. Hence, it is difficult to confirm or refute the chosen curves. Nonetheless a shift in the curves might impact the condensation fluxes, especially for the filtration of SSA, which is important as it contains reactive sodium, which acts as the limiting reactant in these examples, for forming $Na_2SO_4$. A sensitivity analysis was carried out to estimate the impact of a change of the filter efficiency curves. To do this, the efficiency curves were shifted up as shown in Fig. 6. The G2 efficiency curve (red) was fully shifted up by 1%, and the 3 others were shifted up only where it was possible without having an efficiency exceeding 100% (e.g., between a particle size of 0.03 µm and 0.6 µm for E11 and E12, and between 0.01 µm and 2.6 µm for M6). The impact of filtration curve changes on the new amount of particles passing through the filters was estimated.

It was found that a shift of 1% of the efficiency curves had a major effect on the overall volume of contaminant injected. For the standard filtration system (G2, M6 and E11) contaminants particles volume decreased by 8.9%. Concerning HEPA filtration system; the impact was bigger with a decrease of contaminant level up to 16.1%.

**Table 9** Dew point of $Na_2SO_4$ at the four stages of the turbine with G2, M6 and HEPA filtration system

| | Filtration system | $Na_2SO_4$ dew point (K) |
|---|---|---|
| Stage 1 NGV | G2, M6 | X + 32 |
| | HEPA | – |
| Stage 1 blades | G2, M6 | X + 167 |
| | HEPA | X + 37 |
| Stage 2 NGV | G2, M6 | X + 152 |
| | HEPA | X + 42 |
| Stage 2 blades | G2, M6 | X + 97 |
| | HEPA | X + 77 |

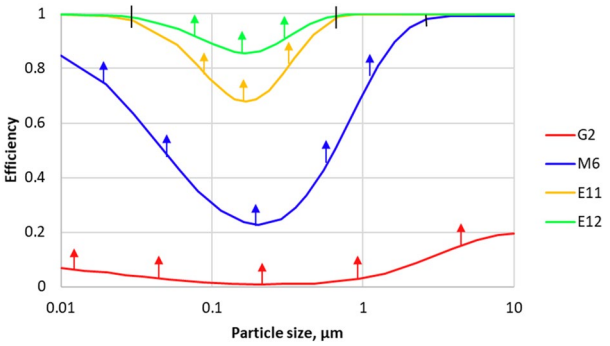


**Fig. 6** Illustration of the shift of the efficiency curves by 1%

## 14 Choice of input

The relevant parameters chosen as gas turbine inputs are discussed in this Section. The impact of these choices (such as air characteristics, SSA model, dust chemistry, etc.) have been evaluated along with the choice of the condensation fluxes model.

## 15 Sea salt aerosol input

SSA concentration in atmosphere, as well as the size distribution, is season dependant [21]. Humidity, also, plays a large role in the phase of the sea salt and the size of the aerosol particles. When the humidity is above 70%, SSA absorbs the moisture in the air and the particles diameter increases [21, 32]. The relative humidity in the Persian Gulf oscillates around 80% [43]. In addition, SSA size decreases with the altitude, as the smallest particles go at higher altitude than big and heavy particles [21]. The size distribution has been measured at 10 m above the seawater, and the bottom of the platform was at 14 m above the seawater. Hence, looking at Fig. 7, it can be deduced that there is from 25 to 36% less SSA at 14 m. However, the top of the platform reaches 28 m above the seawater, with a SSA concentration that correspond to 38% of the SSA concentration at 14 m. Moreover, smaller particles are expected at 28 m height, between 10 and 20 µm.

Most of the trace elements do not have a significant impact, however, species such as vanadium can be harmful to gas turbine component [44]. In fact, similarly to sodium sulphate or potassium sulphate, molten vanadates (for example sodium vanadyl vanadate, $Na_2O.V_2O_4.5V_2O_5$) can dissolve the oxide scales and thus accelerates the diffusion of oxygen and sulphides to the metal substrate [45]. In addition, sodium vanadyl vanadate melts at a relatively low temperature 550 °C [46]. If vanadium amount was taken into consideration in the simulations, it would have represented about $10^{-11}$% of the atomic total for MTData input (mol) considered in the whole simulations. Nonetheless some vanadates could be able to form. In addition, vanadium can be also contained in fuel, even with the tight restrictions in place [44]. Hence, the gas turbine could suffer

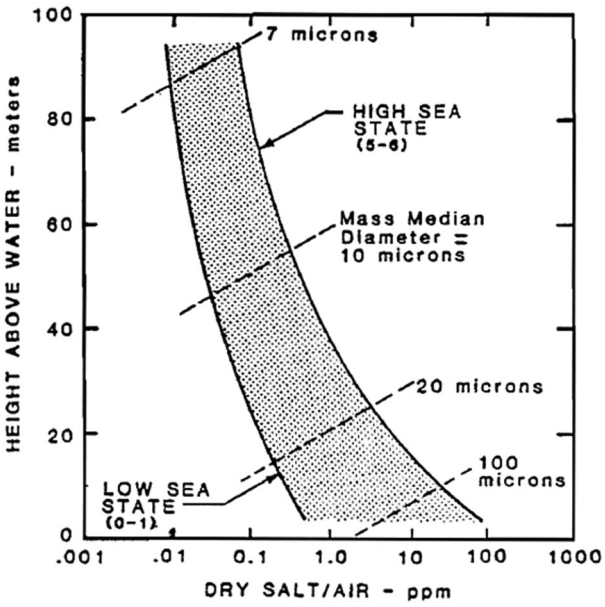


**Fig. 7** Generalized characteristics of salt aerosol boundary layer above water/ air interface [21]

over time with severe damage caused by vanadium-induced hot corrosion, coming from both sea salt and natural gas, which could accumulate and impact gas turbine lifetime.

## 16 Impact of pressure

Gas turbines run at higher pressure than 1 atm (the pressure of the hot gas stream at the output of the turbine section). Inside the turbine itself, the pressure is higher depending on the location. Case C–G2,M6 has being evaluated at different pressures (7.8, 7.99, 15.2 and 16.42 atm/7.9, 8.1, 15.4 and 16.64 bar respectively).

It was observed that the change of pressure did not impact the species present in the hot gas stream, but does impact the partial pressure of the species in the gas. The evolution of the partial pressure of $Na_2SO_4$ dependence on the hot gas stream absolute (local) pressure is plotted in Fig. 8. This means that with the real pressures in the turbine section, deposits are higher than the ones calculated at 1 atm, and corrosion rates would be expected to be higher. In addition, the different stages have different pressures, hence different fluxes.

## 17 Conclusions

The impact of the environment on corrosive species condensation rate was evaluated. Many contaminants can enter the gas turbine and damage the blades. Contaminants from atmospheric pollution (corrosive gas or $H_2S$), atmospheric dust,

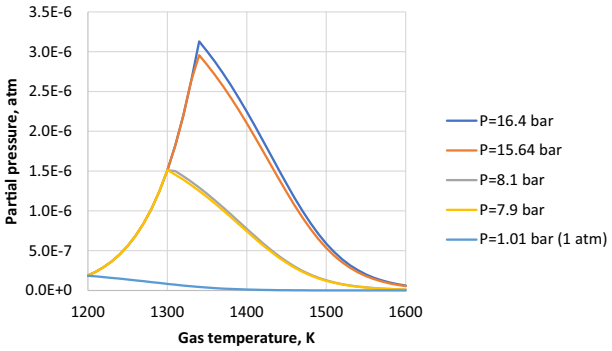


**Fig. 8** Partial pressure of Na2SO4 for case C–G2, M6 at different hot gas stream pressures

sea salt and Saharan dust were studied. It was found that most of the sulphur content comes from the natural gas, but the amount coming from the corrosive gas (in the atmosphere or around the offshore platform) can reach up to 22% when $H_2S$ levels are over 200 ppm. However, it was found that the sodium was the limiting reactant, meaning sulphur is present in excess. The filtration system is able to catch sulphur associated sea salt and Saharan dust, but not from the corrosive gas and the natural gas. In addition, a filtration system has a direct impact on sodium amount and, as consequence, on the sodium sulphate amount in the turbine. Sea salt aerosol and Saharan dust have a wide range of sizes ranging from less than 0.01 µm–100 µm. That implies that effective filters must be able to catch both tiny particles and big particles, while keeping in mind that increasing the efficiency also increases the pressure losses.

MT Data software predicted the presence of many condensed, species especially $Na_2SO_4$, which might be detrimental to gas turbines. It also predicted the presence of $K_2SO_4$ when potassium was recorded in sea salt. Furthermore, the software predicted a presence of solid species that do not damage blades by hot corrosion but might cause damage by erosion. These solid species are, for example, oxides ($Al_2O_3.2H_2O$, $Fe_2O_3$, $Al_2O_3$, $Fe_3O_4$, $Al_{12}CaO_{19}$, $CaFe_2O_4$), sulphates ($MgSO_4$, $Al_2(SO_4)_3$, $Fe_2(SO_4)_3$, $CaSO_4$,) or silicates ($Al_2O_3.SiO_2$, $CaO_3Si$, $CaAl_2Si_2O_8$, $Al_2Na_2SiO_{16}$, $SiO_2$).

Fluxes of deposition of corrosive species directly depends on the partial pressure of these species. It was found that the fluxes are higher at stage 2 NGV of the turbine than the three other ones. The higher the condensation flux of $Na_2SO_4$, the higher the corrosion rates are expected to be. Hence, the lifetime of these components is lowest when the least efficient filtration system (G2, M6; case 3.h-G2, M6) is used. The conclusions from this work would form a useful background to try and estimate the extent of the corrosion damage on turbines' blades. The application of this approach, in conjunction with more sophisticated Fluid Dynamics models, could help shed some lights on the problem of modelling the dependence of corrosion damage to fuel and air chemistry.

**Data Availability** Data supporting this study cannot be made available due to commercial sensitivity reason.

## Declarations

**Conflict of interest** The authors do not have any conflict of interest.



## References

1. Department for Business E& IS. UK Energy in Brief 2022. London: 2022.
2. TMI Staff and Contributors. Worldwide Gas Turbine Report. Turbomachinery International 2020.
3. EDF. Combined cycle gas turbine power plants n.d.
4. Polyzakis, A.L., Koroneos, C., Xydis, G.: Optimum gas turbine cycle for combined cycle power plant. Energy Convers. Manage. **49**, 551–563 (2008). https://doi.org/10.1016/J.ENCONMAN.2007.08.002
5. Poullikkas, A.: An overview of current and future sustainable gas turbine technologies. Renew. Sustain. Energy Rev. **9**, 409–443 (2005). https://doi.org/10.1016/J.RSER.2004.05.009
6. Gurrappa I, Yashwanth IVS, Mounika I, Murakami H, Kuroda S. The importance of hot corrosion and its effective prevention for enhanced efficiency of gas turbines. gas turbines—materials, modeling and performance, 2015. https://doi.org/10.5772/59124.
7. Sumner, J., Encinas-Oropesa, A., Simms, N.J., Oakey, J.E.: High temperature oxidation and corrosion of gas turbine materials in burner rig exposures. Mater. Sci. Technol. **29**, 813–821 (2013). https://doi.org/10.1179/1743284712Y.0000000097
8. Gialanella, S., Malandruccolo, A.: Aerospace Alloys (2020). https://doi.org/10.1007/978-3-030-24440-8
9. Srinivasachar, S., Helbe, J., Ham, D., Dumazetis, G.: A kinetic description of vapor phase alkali transformations in combustion systems. Prog. Energy Combust. Sci. **16**, 303–309 (1990)
10. Kleinhans, U., Rück, R., Schmid, S., Haselsteiner, T., Spliethof, H.: Alkali vapor condensation on heat exchanging surfaces: laboratory-scale experiments and a mechanistic CFD modeling approach. Energy Fuels **30**, 9793–9800 (2016). https://doi.org/10.1021/acs.energyfuels.6b01658
11. Lide DR. CRC Handbook of Chemistry and Physics. CRC Press LLC; 1997.
12. Perry, R.H.: Perry's chemical engineers' handbook, 6th edn. McGraw-Hill, New York (1984)
13. Orhon D, Kurz R, Hiner SD, Benson J. Tutorial - Gas Turbine Air Filtration Systems for Offshore Applicatoin. Houston, Texas: 2015.
14. Denjean, C., Cassola, F., Mazzino, A., Triquet, S., Chevaillier, S., Grand, N., et al.: Size distribution and optical properties of mineral dust aerosols transported in the western Mediterranean. Atmos. Chem. Phys. **16**, 1081–1104 (2016). https://doi.org/10.5194/acp-16-1081-2016
15. Kaaden, N., Massling, A., Schladitz, A., MüLLER, T., Kandler, K., SchüTZ, L., et al.: State of mixing, shape factor, number size distribution, and hygroscopic growth of the Saharan anthropogenic and mineral dust aerosol at Tinfou, Morocco. Tellus B **61**, 51–63 (2009). https://doi.org/10.1111/j.1600-0889.2008.00388.x
16. Schütz, L., Jaenicke, R., Pietrek, H.: Saharan dust transport over the North Atlantic Ocean. Special Papers—Geol Soc Am **186**, 87–100 (1981)
17. Stohl, A.: Intercontinental transport of air pollution. Springer-Verlag, Berlin Heidelberg (2004)

18. Hamdi-Aissa B, Valles V, AVENTURIER A, Ribolzi O. Soils and Brine Geochemistry and mineralogy of hyperarid desert Playa, Ouargla Basin, Algerian Sahara. Arid Land Research and Management 2010; April–June:103–26. https://doi.org/10.1080/1532480490279656.
19. Athanasopoulou E, Protonotariou A, Papangelis G, Tombrou M, Mihalopoulos N, Gerasopoulos E. Long-range transport of Saharan dust and chemical transformations over the Eastern Mediterranean. Atmosp Environ 2016;140:592–604. https://doi.org/10.1016/j.atmosenv.2016.06.041.
20. Soares, C.: Gas turbines, 2nd edn. Butterworth-Heinemann, Oxford, UK (2014)
21. Wilcox M, Baldwin R, Garcia-Hernandez A, Brun K. Guideline for Gas Turbine Inlet Air Filtration Systems RELEASE 1.0. 2010.
22. BS EN ISO 16890–1:2016—Air filters for general ventilation. Technical specifications, requirements and classification system based upon particulate matter efficiency (ePM) n.d. https://shop.bsigroup.com/ProductDetail/?pid=000000000030357254. Accessed July 13 2021.
23. British Standards Institution. High efficiency air filters (EPA, HEPA and ULPA). : Part 1, Classification, performance testing, marking n.d.:17.
24. Wilcox M, Kurz R, Brun K. Technology review of modern gas turbine inlet filtration systems. Int. J. Rotating Mach. 2012:15. https://doi.org/10.1155/2012/128134.
25. Orhon D, Van Der Kaag J, Taylor S. Impact of EPA Air Intake filtration on gas turbines operating in middle east offshore applications and fueled with sour gas. the future of gas turbine technology. In 8th International Gas Turbine Conference, Brussels, Belgium: 2016.
26. Alebić-Juretić A, Čanić KŠ, Kavčič I, Klai ZB. The Saharan sand episode on 12th of April 2002 in the northern Adriatic area, Croatia. In: Proceedings of the 15th International Conference on Harmonisation within Atmospheric Dispersion Modelling for Regulatory Purposes, 2013.
27. Mahowald, N., Albani, S., Kok, J.F., Engelstaeder, S., Scanza, R., Ward, D.S., et al.: The size distribution of desert dust aerosols and its impact on the Earth system. Aeol. Res. **15**, 53–71 (2014). https://doi.org/10.1016/j.aeolia.2013.09.002
28. Clapeyron E. Mémoire sur la puissance motrice de la chaleur. Journal de l'Ecole Polytechnique 1834;XIV:153–90.
29. Tomeczek, J., Palugniok, H., Ochman, J.: Modelling of deposits formation on heating tubes in pulverized coal boilers. Fuel **83**, 213–221 (2004). https://doi.org/10.1016/S0016-2361(03)00219-9
30. Lewis ER, Schwartz SE. Sea Salt Aerosol production: mechanisms, methods, measurements, and models. Am. Geophys. Union; 2004.
31. Kaloshin, G.A., Grishin, I.A.: An aerosol model of the marine and coastal atmospheric surface layer. Atmos. Ocean **49**, 112–120 (2011). https://doi.org/10.1080/07055900.2011.581548
32. O'Dowd CD, Smith MH, Consterdine IE, Lowe JA. Marine aerosol, sea-salt, and the marine sulphur cycle: a short review. Atmospheric Environment 1997;31:73–80. https://doi.org/10.1016/S1352-2310(96)00106-9.
33. Naeli R. The effect of seawater on the interfacial tension: smart water flooding. Second International Conference in New Research on Chemistry and Chemical Engineering. Dubai; 2016.
34. Orhon D, Van Der Kaag J, Taylor S, Impact of EPA air intake filtration on gas turbines operating in middle east offshore applications and fueled with sour gas, 8th International Gas Turbine Conference, 12th—13th October 2016, Brussels, Belgium.
35. International Organization for Standardization. ISO 6976 Natural gas—Calculation of calorific values, density, relative density and Wobbe index from composition. 1995.
36. Gilliland, E.R.: Diffusion coefficients in gaseous systems. Ind. Eng. Chem. Res. **26**, 681–685 (1934). https://doi.org/10.1021/ie50294a020
37. Kutatela SS. Foundations of the theory of heat transfer. Atomizdat 1979.
38. Brown KL, Wray S. 7—Control of airborne contamination in food processing. In: Lelieveld HLM, Holah JT, Napper DBT-H in FP (Second E, editors., Woodhead Publishing; 2014, p 174–202. https://doi.org/10.1533/9780857098634.2.174.
39. Kowalski WJ, Bahnfleth W. MERV Filter Models For Aerobiological Applications. Air Media 2002.
40. Brekke O, Bakken LE, Syverud E. Filtration of gas turbine intake air in offshore installations: the gap between test standards and actual operating conditions 2009:371–9. https://doi.org/10.1115/GT2009-59202.
41. Gong, S.L., Barrie, L.A.: Modeling sea-salt aerosols in the atmosphere. J. Geophys. Res. **102**, 3805–3818 (1997)
42. Toba, Y.: On the giant sea-salt particles in the atmosphere. Tellus **17**, 365–382 (1965). https://doi.org/10.3402/tellusa.v17i3.9065
43. eldoradoweather.com. El Dorado Weather—Current Middle East Humidity 2020.

44. Nicholls JR, Simms NJ. 1.20—Gas Turbine oxidation and corrosion. In: Cottis B, Graham M, Lindsay R, Lyon S, Richardson T, Scantlebury D, et al., editors., Oxford: Elsevier; 2010, p. 518–40. https://doi.org/10.1016/B978-044452787-5.00026-3.
45. Lai GY. High-temperature corrosion and materials applications. ASM International; 2007.
46. Singh, H., Puri, D., Prakash, S.: An overview of Na2SO4 and/or V2O5 induced hot corrosion of Fe- and Ni-Based superalloys. Rev. Adv. Mater. Sci. **16**, 27–50 (2007)